J. Chem. Chem. Eng. 7 (2013) 653-665

Cutting Behavior of Acrylic Thick Sheet Subjected to Squared Punch Shearing

Pusit Mitsomwang and Shigeru Nagasawa*

Department of Mechanical Engineering, Nagaoka University of Technology, Niigata 940-2188, Japan

Received: April 18, 2013 / Accepted: May 10, 2013 / Published: July 25, 2013.

Abstract: This paper describes the cutting behavior of a 1 mm thickness acrylic worksheet sheared by a squared punch/die apparatus. In the shearing experiment, a load cell and a high speed camera were used for investigating the shearing load response and the deformation behavior of the worksheet. It was found that the mechanical parameters, i.e., the punch-die clearance and the feed velocity of the punch, affected the shearing load response, the cracks initiation behavior and the separation capability of the worksheet. Additionally, a FEM (finite element method) analysis simulating a two dimensional shearing deformation was carried out in order to investigate the influence of punch-die clearance on the failure patterns. Through this simulation, it was revealed that the punch-die clearance remarkably affected the tensile state of stress concentrated in the sheared zone and the crack initiation behavior of the worksheet.

Key words: Acrylic, shearing, die cutting, cracking, fem analysis.

1. Introduction

A punch-die shearing and/or cutting is a very important process in sheet material forming industry. This process possesses advantages such as providing a high precision sizing of worksheet and a high productivity under a low operation cost.

There are many research works for the shearing process of various metallic sheets. The quality of the sheared-edge profiles is in general characterized by several mechanical factors, such as the punching velocity, the shape and clearance of tools (a punch and dies) and the material properties of the worksheet. In that process, the shearing load, the separation capability and the sheared edge of products vary according those mechanical factors [1, 2].

The shearing process is not only applied to metallic sheets but also to polymer sheets. In researches about the shearing of various resin material worksheets (PP (propylene), PS (polystyrene) and PVC (polyvinylchloride)), the cutting clearance, the tool wear and the punching velocity affected the maximum shearing force [3]. In the cases of PP, PVC and PC films sheared by a cylindrical punching, the generation of a smooth-sheared surface was attributed to a certain small clearance [4].

Many research works have focused and reported on the shearing process of ductile sheet materials [5-7], while some studies of fragile amorphous materials [8, 9] subjected to a squared-punch shearing are still limited to an elementary level. Namely, there are not almost any researches which theoretically clarify the behavior of cracks in the fragile worksheet. Owing to the lack of understanding in the shearing behavior of a fragile worksheet, there are many difficulties to successfully shear and produce a smart profile on a fragile sheet product.

In order to promote the shearing technology for fragile worksheets, and to reveal the effects of mechanical conditions such as the punch-die clearance, the feed velocity of punch, the tool-edge geometry, tool wear and so on, the shearing characteristics and

*Corresponding author: Shigeru Nagasawa, Professor/ Ph.D., research fields: material processing and manufacturing. E-mail: snaga@mech.nagaokaut.ac.jp.

the failure prediction of the worksheet at the sheared zone are highly necessary.

Therefore, in this study, in order to reveal the shearing behavior of a fragile resin worksheet [10], an AC (acrylic) thick worksheet was chosen as a specimen and the two dimensional, squared punch die shearing of the worksheet was experimentally and numerically carried out.

2. Experimental Analysis

2.1 Specimen and Experimental Method

An AC (acrylic) worksheet of thickness t_S = 1 mm was used for the experimental investigation. In order to determine the in-plain mechanical properties of the worksheet, the AC worksheet was inspected by the tensile testing based on the JIS-K7127.

Fig. 1 shows an example of the true stress-true strain diagram of the AC worksheet and its in-plain mechanical properties are shown in Table 1. The AC worksheet was prepared as a rectangular-formed specimen which had a length of L = 70 mm and a width of B = 20 mm. A die-set with two-dimensional squared punch and dies was stacked on a press machine and used for cutting off the worksheet.

Fig. 2 shows a schematic of the shearing apparatus in configuration with the worksheet (specimen). The punch and dies were made of the cold-work tool steel (JIS-SKD11) which had a hardness of 58~60 HRC. The die-set consists of four parts: the center punch, the left/right dies, the left/right strippers and the counter punch. During the downward motion of the punch, the movement of the strippers and the counterpunch was determined by the corresponding springs. The spring constants of the left/right strippers and the counter punch were 5.0 N·mm^{-1} and 4.5 N·mm^{-1}, respectively.

The punch was pushed downward into the die cavity by the servo cylinder of the press machine until the AC worksheet was completely separated. The cutting force F was measured by a load cell which was attached to the moveable cylinder. The cutting line force $f = F/(2B)$ kN·m^{-1} was calculated with respect to the normalized indentation depth d/t_S. A high speed camera was installed for observing the sheared zone of the worksheet.

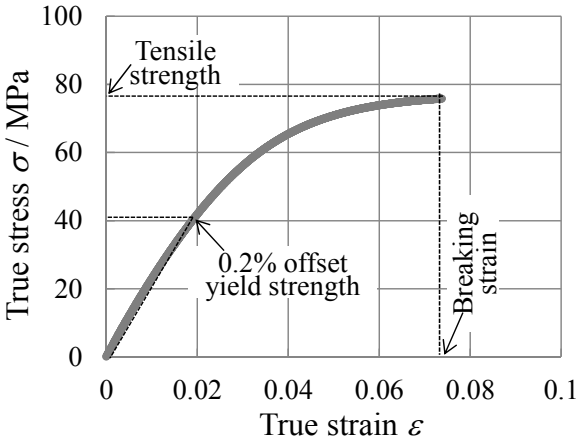

Fig. 1 True stress-true strain curve of the AC.

Table 1 In-plane mechanical properties of AC worksheet.

Thickness: t_S = 1.0 mm, strain rate = 0.002 s^{-1}			
Young's modulus / MPa	Yield strength (0.2% off set) / MPa	Tensile strength / MPa	Breaking true strain
2216	41	75	0.07

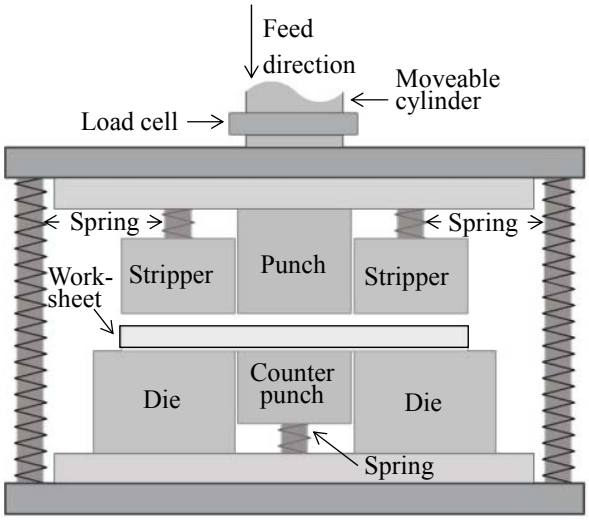

Fig. 2 Schematic of the experimental system.

The friction coefficients between each contacted interface were measured by the horizontal method based on the JIS-P8147. The measured results are shown in Table 2.

Table 2 Friction coefficients between AC and tools.

Combination of tool-AC worksheet	Friction coefficient
Punch-AC, μ_P	0.21 (0.20~0.22)
Die-AC, μ_D	0.21 (0.20~0.22)
Stripper-AC, μ_S	0.28 (0.27~0.30)
Counter punch-AC, μ_C	0.23 (0.22~0.23)
Testing conditions : the horizontal method, applied pressure : 5.84 kPa	

In order to experimentally investigate the shearing behavior of the worksheet, the punch-die clearance ratio c/t_S was chosen as –0.025 (negative clearance), 0.025, 0.05 and 0.1 (positive clearance). Fig. 3 shows the definition of the positive and negative clearances. The feed velocity of punch V was chosen as 0.025, 0.05, 0.25 and 0.5 mm·s^{-1} in this experiment. The shearing experiment was carried out 10 times for each condition.

2.2 Experimental Results

2.2.1 Effect of Punch-Die Clearance

To investigate the effect of the punch-die clearance c/t_S on the cutting characteristics of the worksheet, the feed velocity of punch V was chosen as 0.05 mm·s^{-1}. Fig. 4 shows the relationship between the cutting line force f kN·m^{-1} and the normalized indentation depth of punch d/t_S when varying c/t_S. The indentation depth d/t_S was defined to be zero when the lower surface of the main punch contacted the upper surface of the worksheet. In the early stage $d/t_S \le 0.2$, the gradients $\partial f/(\partial d/t_S)$ for all cases of c/t_S were not significantly different between each other. Regarding the cutting line force, the first peak point f_{P1} occurred at $d/t_S \approx 0.2$, and a wavy load response was observed for $0.2 \le d/t_S \le 0.4$, while there was a secondary peak point f_{P2} at d/t_S 0.5~0.6. Seeing the breaking position d_B/t_S in the case of $c/t_S = -0.025$, it was found that the worksheet was broken at $d_B/t_S \approx 0.45$ which was earlier than the breaking position of 0.5~0.57 for the positive clearance c/t_S = 0.025~0.1.

From the cutting line force shown in Fig. 4, the magnitude of f_{P1} for c/t_S was plotted in Fig. 5, and the

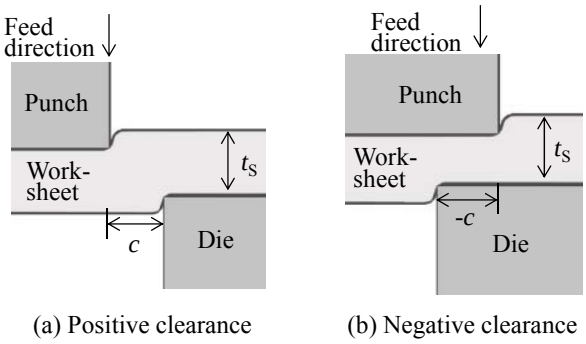

(a) Positive clearance (b) Negative clearance

Fig. 3 Definition of clearance state for punch and dies.

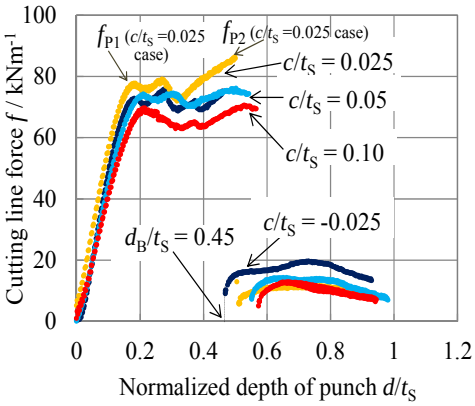

Fig. 4 Representative cutting line force response for c/t_s (V = 0.05 mm·s^{-1}).

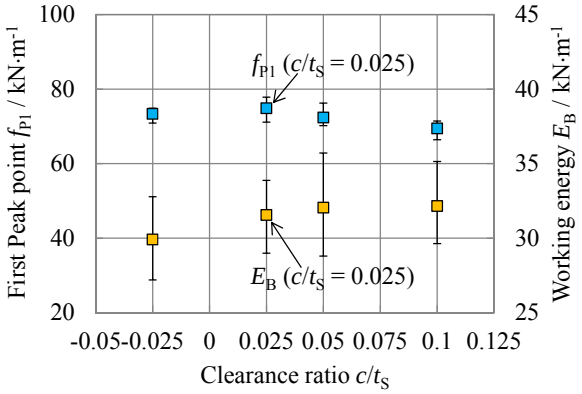

Fig. 5 First peak point and working energy for c/t_s (V = 0.05 mm·s^{-1}, sample = 10 pieces for each c/t_s).

working energy E_B which was calculated from the Eq. (1) was also plotted in this figure.

For the positive clearance, f_{P1} tended to decrease with c/t_S, while that of $c/t_S = -0.025$ was a little lower than that of c/t_S = 0.025. Comparing the working energy E_B for all of the clearance cases, it was found that the energy required for cutting the AC worksheet was lower in the negative case of c/t_S = –0.025,

compared with the positive cases of c/t_S = 0.025, 0.05 and 0.1.

$$E_B = \int_0^{d_B/t_S} f \, \mathrm{d}(d/t_s) \quad (1)$$

Fig. 6 shows the sheared zone of the worksheet with respect to c/t_S for $d/t_S \geq 0.25$. For all cases of c/t_S, when the punch was indented into the worksheet with a small indentation $d/t_S \approx 0.25$, the two primary cracks were initiated near the corner of the tools (punch and dies). These primary cracks propagated as the indentation proceeded. When the indentation of the punch reached a certain range $0.35 \leq d/t_S \leq 0.5$, the propagation of the primary cracks appeared to be stopped. Then, the secondary crack was initiated at the corner of the tools (punch and dies) and propagated in

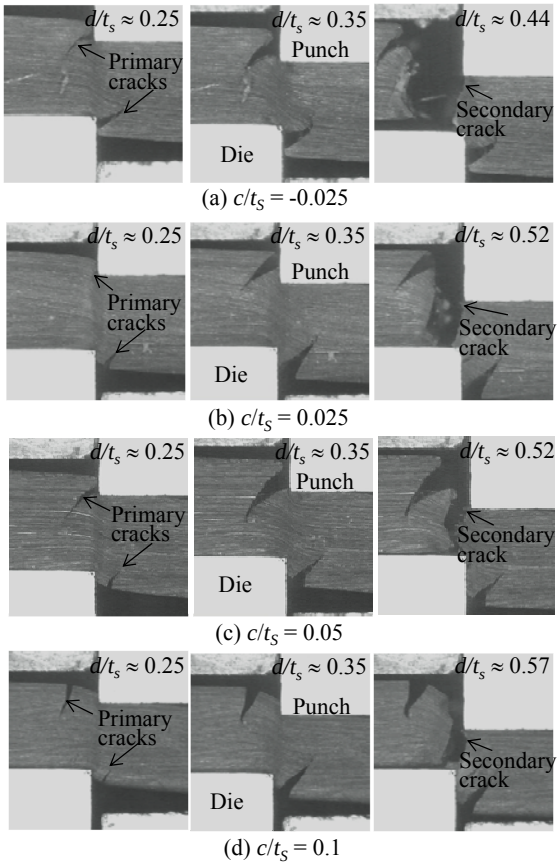

Fig. 6 Side-views of sheared zone of the worksheet with respect to c/t_s (V = 0.05 mm·s^{-1}).

parallel to the shearing direction until the worksheet was completely separated.

From Fig. 6, the patterns of the initiated primary cracks changed remarkably by varying c/t_S and they were classified into several modes. Seeing the side views of the worksheet at the early stage $d/t_S \approx 0.25$, the initiated primary cracks were classified into three patterns as shown in Fig. 7.

In the pattern A, the two primary cracks (upper/lower) were initiated at both the punch and die corners. One of the primary cracks was initiated at the tool corner (punch or dies) while another one was initiated at a location far from the tool corner, in the case of the pattern B. In the case of the pattern C, the two primary cracks were initiated at two points far from the tool corners.

The patterns of initiated primary cracks seemed to be statistically determined by the punch-die clearance c/t_S. Thus, the occurrence probability of the pattern of initiated primary cracks p_i (i = A, B and C) was plotted with respect to c/t_S as shown in Fig. 8.

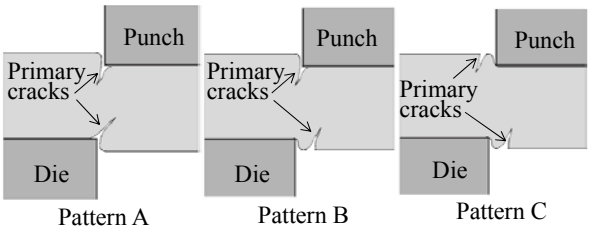

Fig. 7 Representative patterns of the primary cracks initiation.

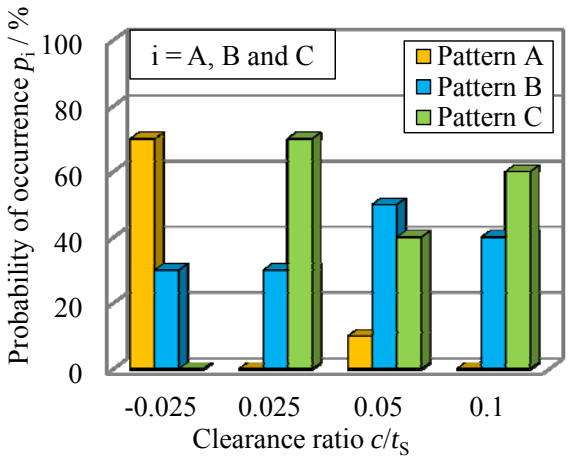

Fig. 8 Probability of the pattern of initiated primary cracks (V = 0.05 mm·s^{-1}, sample: 10 pieces for each c/t_s).

From Fig. 8, it was found that the primary cracks were often initiated at the punch and die corners (the pattern A) when the negative clearance $c/t_S = -0.025$ was used. In the case of positive clearance $c/t_S = 0.025 \sim 0.1$, the pattern C randomly occurred. The pattern B was detected for all the cases of c/t_S.

Regarding the surface cracking at a location far from the tool corners, it was found that the distance between the primary crack position and the tool corner was varied with c/t_S. Namely, the distance was recognized as negative or almost zero for $c/t_S = -0.025$ while the distance was positive and tended to be increased with the positive clearance $c/t_S = 0.025 \sim 0.1$.

When the primary crack propagation was stopped at $d/t_S \approx 0.5$, the secondary crack occurred for $d/t_S > 0.5$ as mentioned above. The secondary crack initiation and its propagation were scarcely different for all the cases of c/t_S.

2.2.2 Effect of Feed Velocity

The effect of the feed velocity V on the shearing characteristics of the AC worksheet was also experimentally investigated. Here, the clearance c/t_S was fixed to be 0.025.

Fig. 9 shows the shearing load responses with respect to V. For $d/t_S \leq 0.2$, the gradient $\partial f/(\partial d/t_S)$ was almost invariant with the velocity V. When V was varied from 0.025 mm·s^{-1} to 0.5 mm·s^{-1}, the first peak line force f_{P1} occurred at the indentation depth $d/t_S \approx 0.2 \sim 0.3$. At the breaking stage $d/t_S \approx 0.5 \sim 0.6$, there were two kinds of load response: (1) a large force drop without any residual resistance and (2) a half sudden and a half residual drop. The former was observed in case of $V = 0.025 \sim 0.05$ mm·s^{-1} while the latter was observed in case of $V = 0.25 \sim 0.5$ mm·s^{-1}. From Fig. 9, the cutting line force and its breaking position d_B/t_S appeared to be affected by V.

Fig. 10 shows the f_{P1} and E_B for the feed velocity V. In the low feed velocity $V = 0.025$ and 0.05 mm·s^{-1}, the working energy E_B was calculated by integrating the Eq. (1) from $d/t_S = 0$ to $d_B/t_S \approx 0.45$, while the

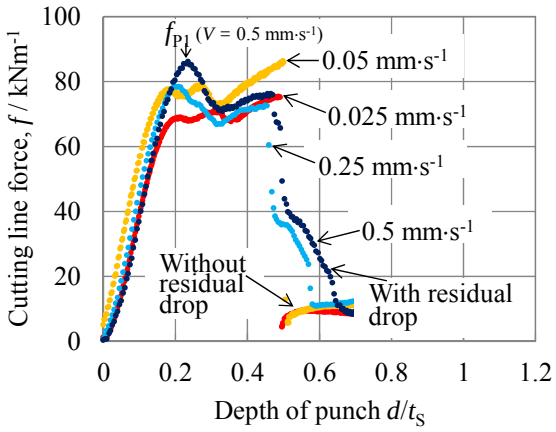

Fig. 9 Representative cutting line force response for V ($c/t_S = 0.025$).

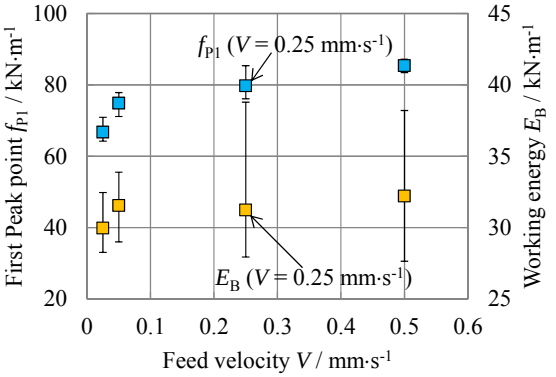

Fig. 10 First peak point and working energy for V ($c/t_S = 0.025$, sample = 10 pieces for each V).

equation was integrated from $d/t_S = 0$ to $d_B/t_S \approx 0.6$ and 0.7 for the case of $V = 0.25$ and 0.5 mm·s^{-1}, respectively. It was found that the magnitude of f_{P1} tended to increase with V, while E_B presents a large dispersion for a range of $V \geq 0.2$ mms^{-1}. The dispersion of E_B remarkably changed when comparing the case of $V < 0.05$ mm·s^{-1}, against $V > 0.25$. This dispersion of E_B was mainly caused by the various-unstable responses of the cutting line force and the corresponding crack propagation in the middle shearing stage $0.25 \leq d/t_S \leq 0.5$.

Fig. 11 shows the side views of the sheared zone of the worksheet by varying V for $d/t_S \geq 0.25$. When the indentation of punch reached $d/t_S \approx 0.25$, the length of the primary cracks was increased with V. The primary crack length for $V \leq 0.05$ mm·s^{-1} was fairly shorter

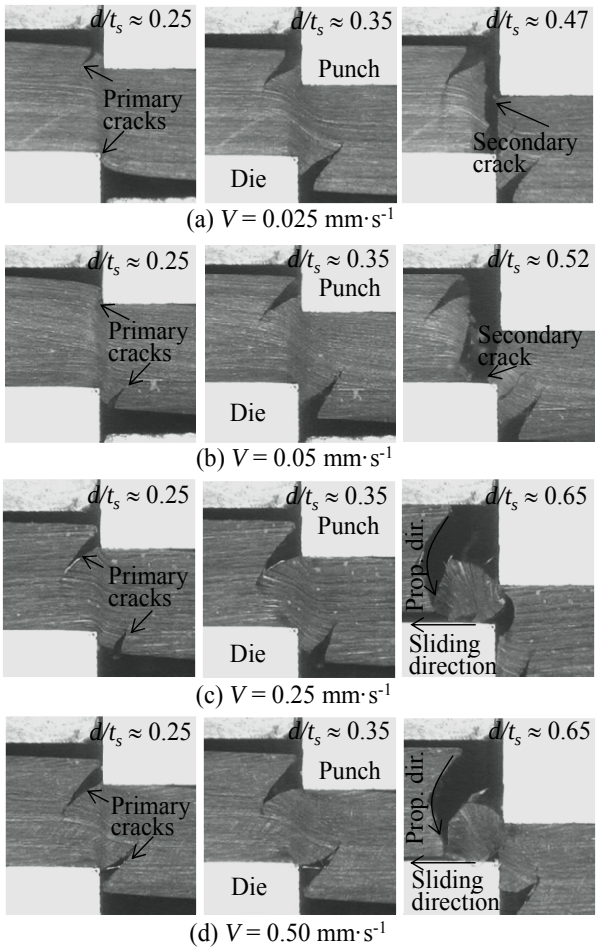

Fig. 11 Side-views of sheared zone of the worksheet with respect to V (for $c/t_S = 0.025$).

than that for $V \geq 0.25$ mm·s^{-1}. This indicates that the propagation of primary cracks was increased by the high feed velocity state for $d/t_S = 0.2$~0.3. Due to the surplus propagation of the primary cracks, the accumulated shearing strain energy on the center of the cutting line appeared to be reduced. This corresponds to the residual drop as shown in Fig. 9. In the case of the high velocity state, the worksheet appeared to slide outward along the die surface and it was gradually separated by the propagation of the primary cracks as shown in Figs. 11c and 11d.

On the contrary, in case of the low velocity state, since the primary cracks were not sufficiently propagated, the accumulated shearing strain energy contributed to cut off the core part of the worksheet (as the secondary shearing). Namely, the secondary

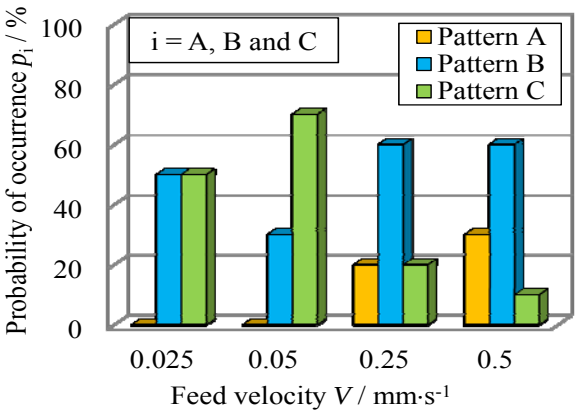

Fig. 12 Probability of the pattern of initiated primary cracks ($c/t_S = 0.025$, sample: 10 pieces for each V).

cracks occurred at the tool corners and propagated until the complete separation of the worksheet. This corresponded to the large drop phenomena without any residual resistance.

Fig. 12 shows the occurrence probability of the pattern of initiated primary cracks with respect to V. Here, the geometrical features on the patterns A, B and C were a little different from the case of Fig. 8. In the case of Fig. 11, the primary cracks occurred just close to the corner of tools, but the additional propagation of the primary cracks changed by the feed velocity. In the case of Fig. 8, the location of initiation was geometrically varied with respect to the clearance c/t_S. Therefore, the geometrical meaning of the three patterns A, B and C must be classified furthermore regarding the feed velocity and the clearance. As shown in Fig. 12, the failure was mainly characterized with the patterns B, C for the low-velocity V = 0.025~0.05 mm·s^{-1}, while the failure appeared to be transferred from the pattern C to the patterns A, B for the high-velocity $V = 0.25$~0.5 mm·s^{-1}.

Through this experimental investigation, authors confirmed that the punch die clearance ratio c/t_S and the feed velocity V affected the cutting load response and the crack behavior of the worksheet.

3. Numerical (FEM) Analysis

According to the experimental result, it was

revealed that the primary crack initiation position was affected by the punch-die clearance c/t_S. To discuss the influence of the punch-die clearance, in this section, the stress distribution in the sheared zone was numerically analyzed at d/t_S = 0.2 (just before the primary cracks occurrence) by varying c/t_S.

3.1 FEM Analysis Conditions

A general-purpose analysis code, MSC.MARC 2010.1.0 was employed to simulate the proposed shearing problem. Fig. 13 shows the two-dimensional shearing FEM model. This model was considered as a large strain problem using the updated Lagrange procedure. The AC worksheet was considered as a squared-form deformable body with a thickness of t_S = 1 mm and a length of l_S = 70 mm. The four-node plain-strain quadrilateral element was used for modeling the worksheet. The fine elements (side length = 50 μm) were used for the shearing zone while the coarse elements were used for the farther zone. These two zones were connected with each other using the glue contact function.

The material property of the worksheet was assumed to be isotropic elasto-plastic with work hardening. This is explained later in the section 3.2. The punch, dies, strippers and counter punch were considered as rigid bodies. Their dimensions were corresponded to the apparatus used for the experimental work. The movement of the strippers and the counter punch was controlled by three sets of springs. The spring stiffness of each stripper k_S and the counter punch k_C were assumed to be 5 and 4.5 N·mm^{-1}, respectively. These values were evaluated from a prior experiment.

During the punch indentation, some elements located in the sheared zone were highly deformed. Consequently, the FEM calculation tended to be fault due to the crushing of several elements. In order to overcome this crushing, the advanced front quad re-meshing function was used. The re-meshing was done when the inner angle of element was greater than

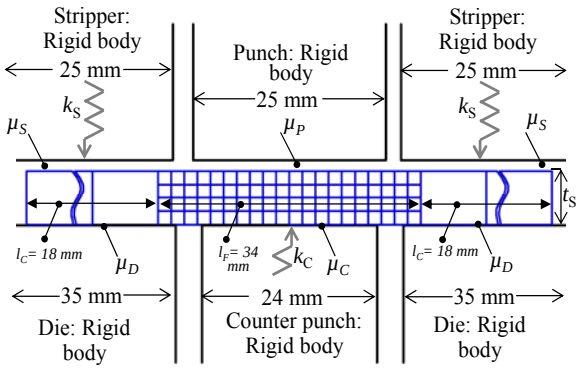

Fig. 13 Schematic of two-dimensional FEM model of shearing deformation.

175º or smaller than 5º. The side length of re-meshing elements was controlled to be approximately 35 μm.

The friction coefficients at the interface of the contacting bodies μ_P, μ_D, μ_U and μ_S were assumed to be 0.2. To define the friction state, the coulomb arc-tangent friction model with a relative slipping velocity threshold of 0.01 was chosen.

In order to investigate the effect of the punch-die clearance c/t_S on the primary cracks initiation position, the c/t_S was chosen as—0.025, 0.025, 0.05 and 0.1. Since there were not any cracks in the experiment before the indentation depth of punch reached $d/t_S \approx 0.2$, any fracture or damage models were not considered here.

3.2 Verification of Constitutive Equation (Material Model)

Regarding the mechanical properties of the AC worksheet, the uni-axial compressive yield strength in the in-plane or in the thickness direction is roughly two times larger than that of the in-plane direction tensile test [11, 12]. Since the AC worksheet at the sheared zone is under compressive state during shearing, the yield strength evaluated from the prior uni-axial tensile test (Fig. 1) must be verified for developing an FEM model. In order to identify a suitable value of yield strength, two linear-hardening material models, Mat. A and Mat. B were proposed and used for the FEM model.

In the case of Mat. A, the yield strength $Y_{S(A)}$ was

41 MPa, which was based on Table 1. $Y_{S(B)}$ = $(2.5 \cdot Y_{S(A)})$ = 102.5 MPa was assumed in the case of Mat. B.

The governing parameters for both material models are shown in Fig. 14 and they were arranged into Table 3.

As shown in Fig. 15, in the case of Mat. A, the gradient of the simulated line force at the shallow depth of punch $d/t_S \leq 0.05$ was similar to the experimental line force. However, the magnitude of the simulated peak point $f_{P1(A)}$ appeared to be too low, compared to the experiment. Regarding this mismatch, $Y_{S(A)}$ seemed to be too low.

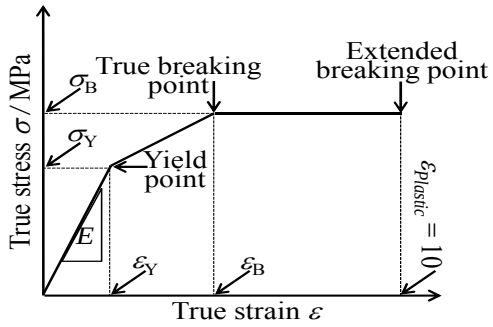

Fig. 14 Stress-strain curve for linear-hardening models.

Table 3 Governing parameters for Mat. A and B.

Model	Parameters			
	E / MPa	σ_Y / MPa, ε_Y	Harden -ing equation	σ_B / MPa, ε_B
Mat. A	2216	41, 0.019	$\sigma_{Plastic} = 582 \cdot \varepsilon_{Plastic}$	75, 0.070
Mat. B		102.5, 0.046		133.5, 0.097

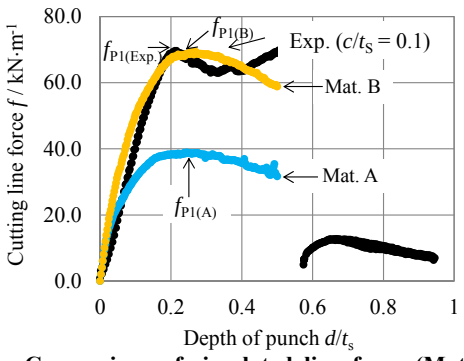

Fig. 15 Comparison of simulated line force (Mat. A, B) and experimental line force ($c/t_S = 0.1$).

In the case of Mat. B, the simulated cutting line force was relatively similar to the experiment for $d/t_S \leq 0.2$. It indicated that the modification of yield strength by using 2.5 times of the tensile yield strength was applicable to the compressive-mode analysis. In the following, the Mat. B was used for simulating.

3.3 Simulation Results and Discussions

Fig. 16 shows the simulated cutting line force for a clearance ratio c/t_S = –0.025, 0.025, 0.05 and 0.1. In the initial shearing stage, $d/t_S \leq 0.05$, the gradient of line force was similar in all of the clearance cases. At the depth of punch $d/t_S \approx 0.2$, a peak line force f_{P1} was observed. For the case of c/t_S = –0.025, 0.025, 0.05 and 0.1, the peak line force f_{P1} slightly decreased with c/t_S, while the peak position d_{P1}/t_S increased with c/t_S. For the early stage, $d/t_S \leq 0.2$, the tendencies of the simulated cutting line force described above appeared to correspond with the experimental results shown in Fig. 4.

For the intermediate depth of punch $d/t_S > 0.2$, the simulated cutting line force dropped in all of the clearance cases, and its behavior was different from the experiment.

Since the upper/lower primary cracks were experimentally initiated and propagated for $d/t_S \geq 0.25$, it was revealed that the simulated cutting line force in the second half stage could not be predicted by using the proposed non-damage FEM model, but the early

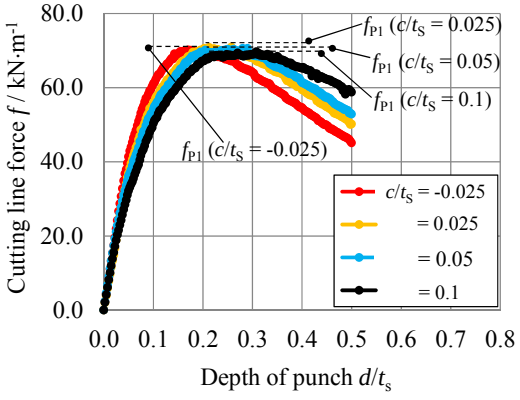

Fig. 16 Simulated cutting line force for c/t_S.

stage and the intermediate stage corresponded well with the experimental results.

Fig. 17 shows some selected vectors of the 1st (maximum) σ_{P1} and 2nd (minimum) σ_{P2} principal stresses in the sheared zone at d/t_S = 0.2. The solid line with diamond-end and circle-end represent the σ_{P1} and σ_{P2} principal stresses, respectively. The red arrows represent the tensile norm of σ_{P1} while the blue arrows represent the compressive norm of σ_{P2}.

Seeing the tensile state of σ_{P1} at the tool corners in the case of c/t_S = –0.025 as shown in Fig. 16a, it was approximately 77 MPa and 72 MPa at the punch and die corners, respectively. Those values of σ_{P1} appeared to be higher than that of c/t_S = 0.025, 0.05 and 0.1 (σ_{P1} ≈ 33~63 MPa for the punch corner and 56~70 MPa for the lower tool corner). This high tensile state illustrated in Fig. 16a, seems to contribute to the generation of the primary cracks near the tool corners when the negative clearance was used.

Fig. 18 shows the magnitude of σ_{P1} as contour band diagrams for c/t_S = –0.025~0.1 at d/t_S = 0.2. From this figure, the following features were revealed: (1) A quite-high tensile state, shown by the gray band (σ_{p1} > 85 MPa = 2.07 $Y_{S(Mat.A)}$), was detected along the center of the sheared zone in all of the cases. (2) This quite-high tensile state zone appeared to be restricted in a narrow zone for c/t_S = –0.025, and it appeared to be suppressed in the vertical direction but slightly expanded in the lateral direction when the clearance c/t_S was increased from 0.025 up to 0.1. (3) Seeing the stress distribution on the free surfaces of the worksheet, a concentrated in-plane tensile stress position, which was roughly located at half of the thickness t_S, was detected on the free surface. The occurrence of this surface tensile stress was clearly seen in the case of c/t_S = 0.025-0.1.

Fig. 19 shows the contour band diagrams of the minimum principal stress σ_{P2} for c/t_S = –0.025~0.1. For all the cases of clearance c/t_S, a high compressive stress state was detected along the center of the sheared zone.

From the side-view photographs of Fig. 5, any cracks were not observed in the central sheared zone for $d/t_S \le 0.25$. The suppression of the cracks at the center of the sheared zone possibly was caused by this high compressive pressure.

Fig. 20 shows the norm of σ_{P1} and σ_{P2} on the worksheet surfaces in the case of c/t_S = –0.025. Figs. 20a and 20b were for the upper surface (along the u-u' axis) and the lower surface (along the l-l' axis),

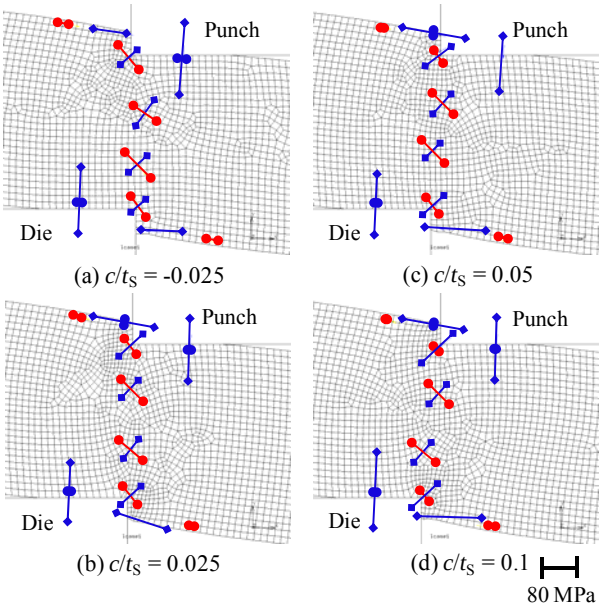

Fig. 17 Vector diagrams of σ_{P1} and σ_{P2} principal stresses (d/t_S = 0.2).

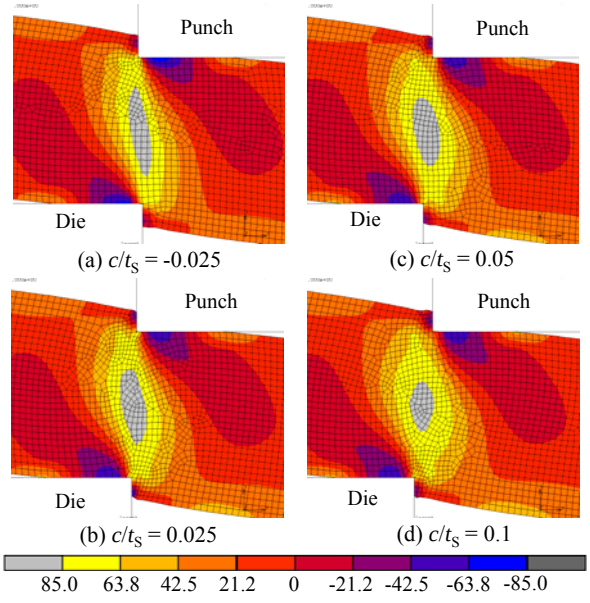

Fig. 18 Contour band diagrams of 1st principal stress σ_{P1} in sheared zone (d/t_S = 0.2).

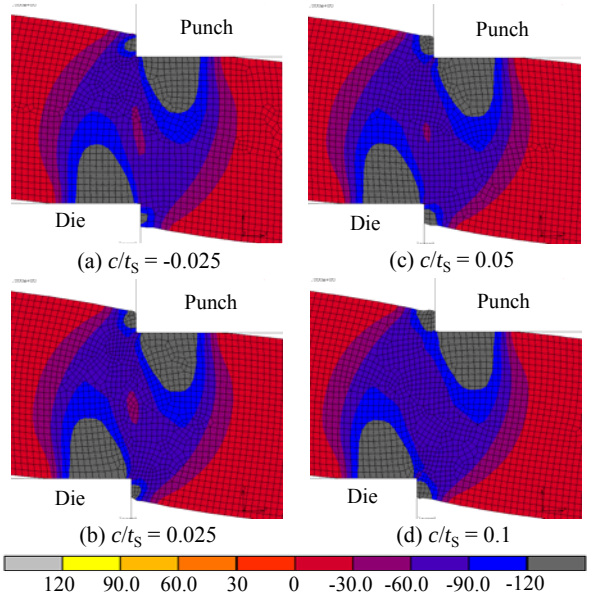

Fig. 19 Contour band diagrams of 2st principal stress σ_{P2} in sheared zone (d/t_S = 0.2).

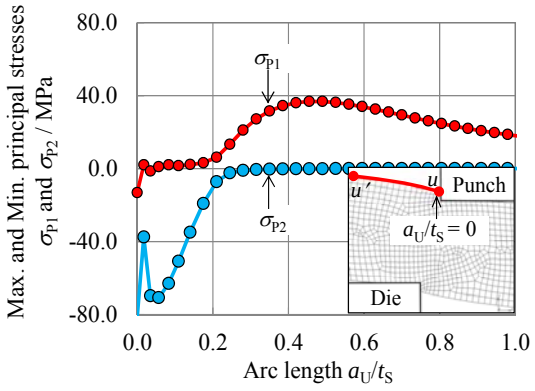

(a) Max. and Min. principal stresses on upper surface

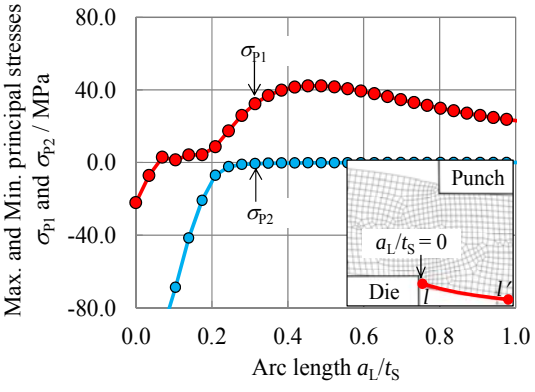

(b) Max. and Min. principal stresses on lower surface

Fig. 20 Magnitude of σ_{P1} and σ_{P2} principal stress on worksheet surfaces (c/t_S = –0.025).

respectively. On both of the surfaces, the stress state was almost in-plane compressible near the side edge of the tools (a_U/t_S and $a_L/t_S \leq 0.1$). The norm of σ_{P1} was increased until the peak point at a_U/t_S and $a_L/t_S \approx$ 0.45~0.5 was reached. After passing through such the peak point, σ_{P1} gradually decreased with a_U/t_S and a_L/t_S as shown in Figs. 20a and 20b.

Since the norms of σ_{P1} and σ_{P2} were remarkably changed at a_U/t_S and $a_L/t_S \approx 0.2$ as shown in Figs. 20a and 20b, the phases of principal axes were transmitted at this point. For the positive clearance cases, the distribution tendency of σ_{P1} and σ_{P2} was almost the same as in the case of negative clearance.

In order to discuss the effect of the clearance ratio on the primary crack initiation position, the norm of σ_{P1} on the worksheet surfaces was plotted. Fig. 21 shows the norms of σ_{P1} for c/t_S = –0.025, 0.025, 0.05 and 0.1. The norms of σ_{P1} were almost invariant for the positive clearance.

In the case of c/t_S = –0.025, as shown in Fig. 21, the norm of σ_{P1} for a_U/t_S and $a_L/t_S > 0.3$ was small, compared to the positive clearance case. This result also indicated that the negative clearance is a superior condition for cutting the fragile AC worksheet, because the occurrence possibility of surface-cracks at a_U/t_S and $a_L/t_S \approx$ 0.45-0.5 would be suppressed.

Fig. 22 shows the experimental and simulated bent angle θ_U on the upper surface, and the angle θ_L on the lower surface. Comparing these experimental and simulated bent angles, the dependency of the clearance c/t_S and the asymmetric bending angles for the lower/upper side were well simulated. It was found that the angles θ_U and θ_L tended to slightly increase when the c/t_s increased from –0.025 to 0.1. Moreover, at the same clearance ratio, the experimental and simulation results revealed that θ_L was always larger than θ_U. Since the large bending deformation occurred on the lower surface of the worksheet, it contributed to increase the tensile state on the worksheet surface as shown in Fig. 21b.

In order to discuss the correlation between the surface peak position of σ_{P1} and the experimental

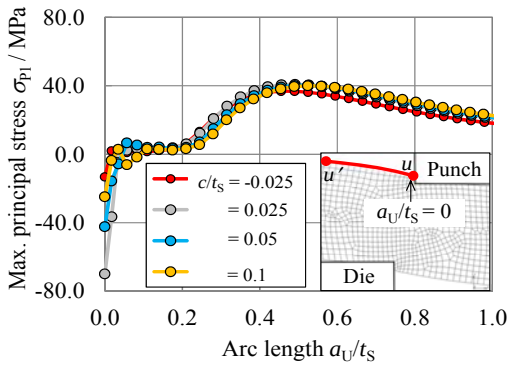

(a) Max. principal stress on upper surface

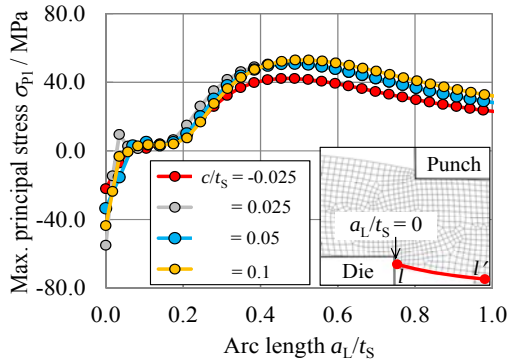

(b) Max. principal stress on lower surface

Fig. 21 Magnitude of the σ_{P1} principal stress on the worksheet surfaces (d/t_S = 0.2).

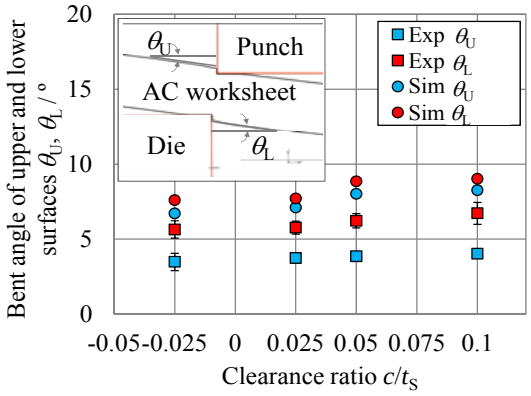

Fig. 22 Bent angle of upper and lower surfaces of worksheet (d/t_S = 0.2).

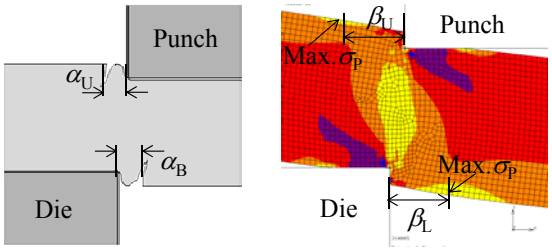

(a) Exp. crack position (b) Peak position of σ_{P1}

Fig. 23 Parameter definition of the α_U, α_L, β_U and β_L.

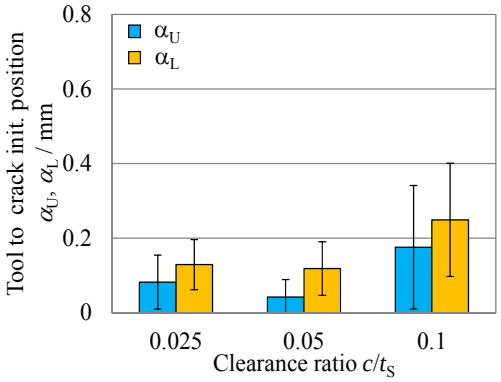

(a) Experimental primary cracks position
(V = 0.05 mm·sec^{-1}, sample = 29 pieces)

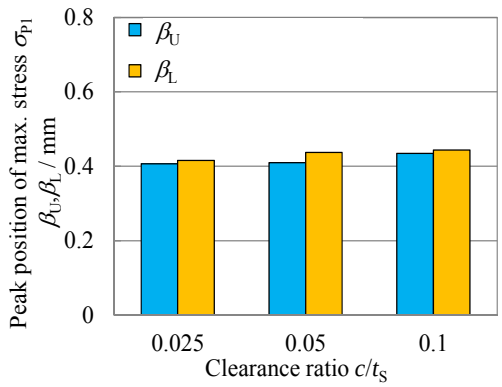

(b) Simulated peak position of σ_{P1}

Fig. 24 Comparison of the primary cracks initiation positions with the peak positions of σ_{P1}.

primary cracks initiation position in the case of positive clearance, the parameters α_U and α_L, defined as the distance between the primary cracks initiation positions and tool corners, shown in Fig. 23a, were measured and compared with the parameters β_U and β_L defined by Fig. 23b (simulated peak position of σ_{P1} on the worksheet surfaces).

Fig. 24a shows the measured results of α_U and α_L while the results of β_U and β_L are shown in Fig. 24b. Comparing Fig. 24b with Fig. 24a, a part of them was fairly similar, especially for the case of c/t_S = 0.1. Namely, the occurrence of the primary cracks seemed to correspond to the peak positions of the surfaces tensile stress.

In the case of positive clearance c/t_S = 0.025, 0.05, the experimental primary cracks initiation position was not supposed to be affected by the peak position of σ_{P1} calculated by the FEM simulation.

4. Prospects

Appropriate failure analysis is furthermore required for predicting the complicated propagation of the primary and secondary cracks. Except for the punch-die clearance and the feed velocity of punch, there are still other factors that control the deformation characteristics of the 1 mm thickness AC worksheet: (a) the edge shape of the punch and dies; (b) the spring stiffness or the suppressed force of the strippers and counter punch. Therefore, a combination of the effect of those factors, including the clearance and feed velocity, should be continuously investigated in order to improve the processing technology to cut fragile materials.

5. Conclusions

A straight punch cutting of a t_S = 1.0 mm thickness (AC) worksheet was experimentally carried out by varying the punch-dies clearance c/t_S and the feed velocity of the punch V in order to reveal the shearing characteristics of the AC worksheet. To discuss with the effect of the punch-die clearance, an FEM simulation was also conducted. Through these works, the followings were derived.

(1) Regarding the experimental results, the punch-die clearance and the feed velocity affected the shearing characteristics, i.e., the shearing load response, the crack initiation, the crack propagation and the cutting ability of the worksheet.

(2) The authors proposed a material model for the AC shearing analysis. In the FEM model, the 2.5 times of the tensile yield strength was assumed. This proposed model was confirmed by a good fit between the simulated cutting line force and experimental cutting line force.

(3) When using the negative punch-die clearance, a high tensile principal stress σ_{P1} occurred at the inside of the worksheet and its surface stress tended to be suppressed. The negative clearance contributed to make the initiation of the primary cracks close to the tool corners and it also contributed to make cut off the worksheet along the central shearing line. To use the negative clearance seemed to be superior for shearing the AC worksheet in smart, compared to the large positive clearance.

(4) In case of a large positive punch-die clearance, such as c/t_S = 0.1, the surface tensile state became a sensitive factor for determining the initiation position of the primary cracks.

(5) The crack propagation pattern presents a transition mode in the middle range of the feed velocity.

Acknowledgments

This work was supported by the JSPS Grants-in-Aid for Scientific Research, Creative and Pioneering Research (c) of Grant Number 25560106.

References

[1] Breitling, J. Process Control in Blanking. *Journal of Materials Processing Technology* **1997,** *71,* 197-192.

[2] Samuel, M. FEM Simulations and Experimental Analysis of Parameters of Influence in the Blanking Process. *Journal of Materials Processing Technology* **1998,** *84,* 97-106.

[3] Jacobs, O. Shear Cutting of thermoplastic Foils. *Polymer Testing* **2003,** *22,* 579-587.

[4] Hojo, H. Shearing of Thermo Plastic Polymer Sheet at Room Temperature. *SOSEI-TO-KAKOU* **1968,** *9,* 304-314.

[5] Maiti, S. K. Assessment of Influence of Some Process Parameters on Sheet Metal Blanking. *Journal of Materials Processing Technology* **2000,** *102,* 249-256.

[6] Klocke, F. Improved Tool Design for Fine Blanking through the Application of Numerical Modeling Techniques. *Journal of Materials Processing Technology* **2001,** *115,* 70-75.

[7] Husson, C. Finite Elements Simulations of Thin Copper Sheet Blanking: Study of Blanking Parameters on Sheared Edge Quality. *Journal of Materials Processing Technology* **2008,** *99,* 74-83.

[8] Nakamura Mfg. Co., Ltd., http://www.nakamuramfg.co.jp/en/introduce/introduce_html (accessed at Oct. 12, 2012).

[9] Xerom Co., Ltd., http://www.Metalstampingxerom.com/metal-stamping/bending/blanking-of-an-amorphous-composite-material (accessed at Oct. 12, 2012).

[10] Crawford, R. J. *Plastics Engineering;* BUTTERWORTH HEINEMANN: Oxford, 1998; p 22.

[11] Kaysons LTD., www.kaysons.in/acrylic/phisicalproperties.pdf (accessed at March 12, 2013).

[12] PARSGLASS Co., http://www.scribd.com/doc/8637812/Acrylic-Material-Data-from-PARSGLASS (accessed at March 12, 2013).